International Journal of Minerals, Metallurgy and Materials
Volume 27, Number 3, March 2020, Page 384
https://doi.org/10.1007/s12613-019-1917-3

Effect of residual structural strain caused by the addition of Co_3O_4 nanoparticles on the structural, hardness and magnetic properties of an Al/Co_3O_4 nanocomposite produced by powder metallurgy

Seyed Rahim Kiahosseini and Hossein Ahmadian

Department of Engineering, Damghan Branch, Islamic Azad University, Damghan 3671639998, Iran

(Received: 10 August 2019; revised: 14 September 2019; accepted: 16 September 2019)

Abstract: Al composites are of interest due to their appropriate ratio of strength to weight. In our research, an Al/Co_3O_4 nanocomposite was generated using a sintering technique. The powders of Al with various Co_3O_4 nanoparticle contents (0wt%, 0.5wt%, 1.0wt%, 1.5wt%, 2.0wt%, and 2.5wt%) were first blended using planetary milling for 30 min, and compressed in a cylindrical steel mold with a diameter of 1 cm and a height of 5 cm at a pressure of 80 MPa. The samples were evaluated with X-ray diffractometry (XRD), scanning electron microscopy (SEM), Vickers hardness, and a vibrating sample magnetometer (VSM). Although the crystallite size of the Al particles remained constant at 7–10 nm, the accumulation of nanoparticles in the Al particle interspace increased the structural tensile strain from 0.0045 to 0.0063, the hardness from HV 28 to HV 52 and the magnetic saturation from 0.044 to 0.404 emu/g with an increase in Co_3O_4 nanoparticle content from 0wt% to 2.5wt%.

Keywords: Residual strain; Vickers hardness; vibrating sample magnetometer; scanning electron microscopy

1. Introduction

A composite material is a macroscopic physical admixture of two or more different compounds [1–2]. Nevertheless, each of the compounds maintain their specifically physicochemical features, which concurrently enhance the whole composite [3]. A composite generally comprises two key compounds, namely a reinforcement (e.g., fibers, particles, laminates, or fillers) and a matrix (e.g., a polymer, metal, or ceramic) [4–5]. The matrix retains the outline of a designed sample, and the reinforcement enhances the mechanical features of the composite [6–7]. With the correct design, the composite features can improve on those of the individual initial raw compounds [8–9].

A nanocomposite is a type of composite that minimally consists of a compound with nanometer dimension (1–100 nm) [10–11]. Additionally, a nanocomposite powder is defined as a composite of different powders with a nanometer dimension [12–13]. Major physical features of a composite are enhanced by reducing the size of particles to the nanometer scale. A prime goal of researchers is to obtain an admixture at molecular dimensions [14–15].

Among metal-based composites, Al-based composites have been the focus of engineers owing to their lightweight and remarkable mechanical and tribological features [16–17]. Al-based composites have wide application in a variety of industries including automobile manufacture and aerospace [18]. The composite features are dependent upon the reinforcement selection and manufacturing technique. The composite can be produced using several procedures, including powder metallurgy. Owing to the low manufacturing cost, ease of use and accuracy in the manufacture of complex geometrical fragments, powder metallurgy has wide application in the fabrication of Al-based composites [19–20]. Important aspects of this technique include mixing, compacting, forming, and curing the fabricated powders of the composite. To generate Al-based composites, a variety of reinforcements are applied to enhance their features. In the current research, Co_3O_4 nanoparticles were embedded in an Al matrix.

Cobalt oxide II and III, Co_3O_4, are black powders that

Corresponding author: Seyed Rahim Kiahosseini E-mail: rkiahoseyni@yahoo.com

have gained interest because of their magnetic features. This spinel oxide has easy accessibility and thermodynamic stability at ambient temperatures and minimal pressure of oxygen [21–22].

Application of novel durable magnetic materials and improvements in their characteristics have received attention for industrial and scientific investigation. The use of magnetic nanomaterials has been extensively examined in different fields including data storing, sensors, catalysts, magnetic resonance imaging, and biomedical applications [23–24]. Among these materials, the use of magnetic Co_3O_4 nanoparticles is highlighted in hypothermia and as a contrast agent applied in magnetic resonance imaging [25]. The inclusion of a reinforcement agent (e.g., Co_3O_4) in a composite can create residual stress and strain in the crystal construct of the matrix [26].

Residual stress is the stress remaining from the construction of materials in the absence of exterior loads. The residual stress stems from the plastic deformation gradient created by processing mechanically or a thermal gradient ascribed to the sample cooling method. As a result, the residual stress and strain can influence the magnetic action of the composite material [27].

The current research aimed to assess the impact of adding magnetic Co_3O_4 nanoparticles to an Al-based composite and, consequently, the influence of residual strain on the Al crystal structure.

2. Experimental

2.1. Materials and method

To generate an Al/Co_3O_4 composite, Al powder were used with 99.999% purity, a melting point of 660ºC, and a quasi-spherical grain size of 1–2 μm, and Co_3O_4 nanoparticle with a melting point of 895ºC and a mean particle size of less than 50 nm were used. Mixtures were prepared by weight to produce nanocomposites with different Co_3O_4 nanoparticle content (Table 1).

The particles were blended according to the predetermined weights and subjected to homogenization in a planetary ball mill with a ball to powder weight ratio of 10 to 1. The total weight of each sample was 11.5 g, and the samples were milled at 250 r/min for 30 min. Finally, composite samples with a diameter of 1 cm and a height of 5 cm with various Co_3O_4 nanoparticle contents (0, 0.5wt%, 1.0wt%, 1.5wt%, 2.0wt%, and 2.5wt%) were compressed in a steel mold at 80 MPa.

Table 1. Weight composition of each material in Al-based composites reinforced by Co_3O_4 nanoparticles

Sample	Al / g	Co_3O_4 / g
Al	11.5000	—
Al/0.5wt%Co_3O_4	11.4425	0.0575
Al/1.0wt%Co_3O_4	11.3850	0.1150
Al/1.5wt%Co_3O_4	11.3275	0.1725
Al/2.0wt%Co_3O_4	11.2700	0.2300
Al/2.5wt%Co_3O_4	11.2125	0.2875

To improve the sample strength, all samples were sintered by heating to 500ºC for 30 min under an Ar atmosphere. The samples were then cooled to 400ºC, and loaded under 10 MPa while cooling to 200ºC to enhance their strength and densification.

2.2. Procedures

The crystal structure of the composite samples was studied via X-ray diffractometry (XRD) at 2θ = 20º–80º, and their crystallite size and residual structural strain were measured using the Williamson-Hall method.

To evaluate the distribution of Co_3O_4 nanoparticles in the Al matrix, micrographs of the samples at 20k magnification were prepared by scanning electron microscopy (SEM). The hardness of the samples was measured by Vickers hardness at 5 points and under s force of 29.4 N that was held for 10 s. The Vickers hardness number was determined according to Eq. (1).

$$\mathrm{HV} = \frac{1000P}{A} \tag{1}$$

where P is the applied force based on kg and A is the contact area of the indent based on mm^2.

The magnetic behavior of the manufactured samples was specified by a vibrating sample magnetometer (VSM). In this technique, vibrating samples were exposed to a magnetic field with constant frequency, and their magnetic parameters were estimated by a coil sense. The hysteresis magnetization was graphed against the magnetic field to determine various parameters including magnetic saturation (M_s), coercivity (H_c), and remanence magnetization (M_r).

2.3. Statistical analysis

To calculate the average value of the examined samples, the acquired data were evaluated with one-way variance analysis (ANOVA). Significant differences between attained averages were determined by Tukey's multiple comparison test at a probability of 95% ($p < 0.05$).

3. Results and discussion

3.1. XRD analysis

Fig. 1 depicts the XRD scans of the Al/Co_3O_4 composite

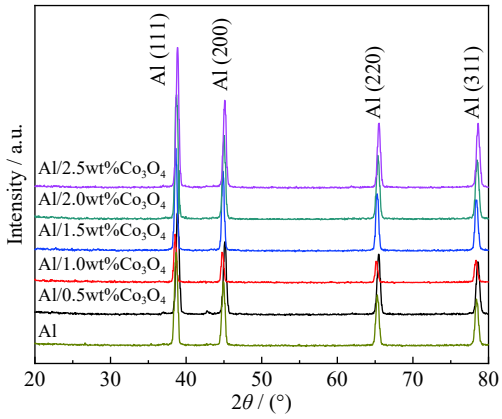

Fig. 1. XRD patterns of Al/Co_3O_4 composites with different contents of Co_3O_4.

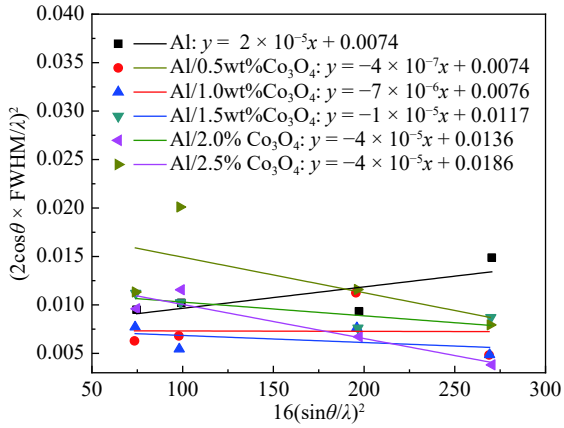

Fig. 2. Plotted graph according to Williamson-Hall method and linear regression of data resulted for Al/Co_3O_4 composite samples with various Co_3O_4 contents.

samples. The peaks belonging to the crystal plane were specified according to PDF2: 00-001-1176 standards.

Based on the XRD observation, the crystallite size and residual strain of the samples were computed with Eq. (2) using the Williamson-Hall approach [28–31]. This procedure was used to determine the Bragg diffraction angle (θ) and full width at half maximum of each peak (FWHM). Based on the X-ray wavelength of the Cu Kα cathode (λ = 0.15406 nm), the graph of $(2\cos\theta\times\text{FWHM}/2)^2$ vs. $16(\sin\theta/\lambda)^2$ was plotted to determine the linear regression of the graph. The crystallite size (D) and structural micro-strain (e) were calculated from the y-intercept and slope of the equation, respectively.

$$\left(\frac{2\cos\theta\times\text{FWHM}}{2}\right)^2=\left(\frac{0.9}{D}\right)^2+16e^2\left(\frac{\sin\theta}{\lambda}\right)^2 \quad (2)$$

Fig. 2 represents the results of the Williamson-Hall equation. Based on the y-intercept obtained from the linear equation between 0.0074 and 0.0186, the Al crystallite size of all samples was approximately 7–10 nm with no substantial differences. This occurrence suggests that the addition of Co_3O_4 and the sintering procedure had no considerable impact on the Al crystallinity. In fact, the incorporated Co_3O_4 nanoparticles filled the interspace of the Al particles.

Fig. 3(a) displays the slopes of the lines fitted according to the Williamson-Hall method. The micro-strain of the Al crystal structure in the absence of Co_3O_4 was in the tensile mode with a value of 0.0045, which changed to the compressive mode with the addition of Co_3O_4. This occurred by accumulation of incorporated particles into the free interspace of Al particles that affected their Al particles and their crystal structure by compressive strain, as shown in the Fig. 3(b). The compressive strain increased with increasing Co_3O_4 (Fig. 3(a)), such that at 2.5wt%, the compressive strain was 0.0063.

3.2. Assessment of the composites using SEM

Fig. 4 shows the results of the assessment of Al/Co_3O_4

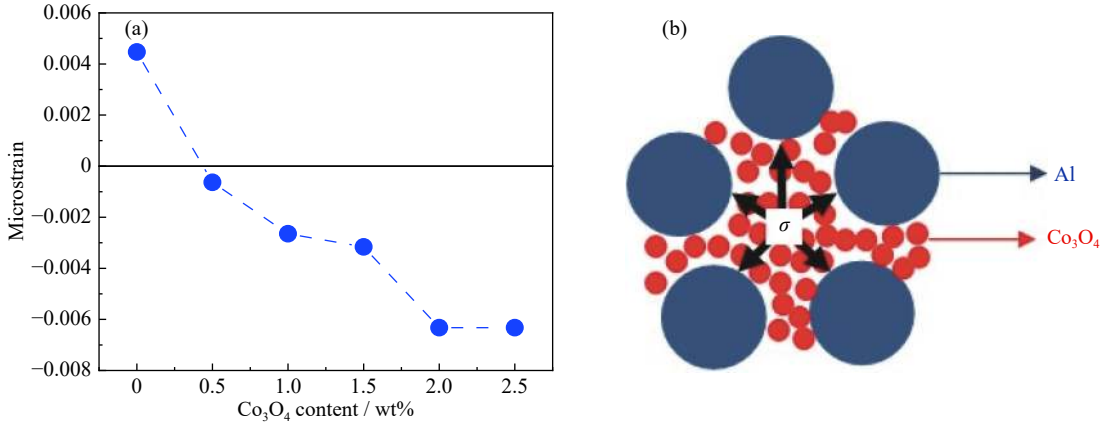

Fig. 3. (a) Microstrain of the Al crystal structure plotted based on Williamson-Hall method attributed to the Al/Co_3O_4 composites with different Co_3O_4 contents; (b) schematic of the interaction between Co_3O_4 and Al particles.

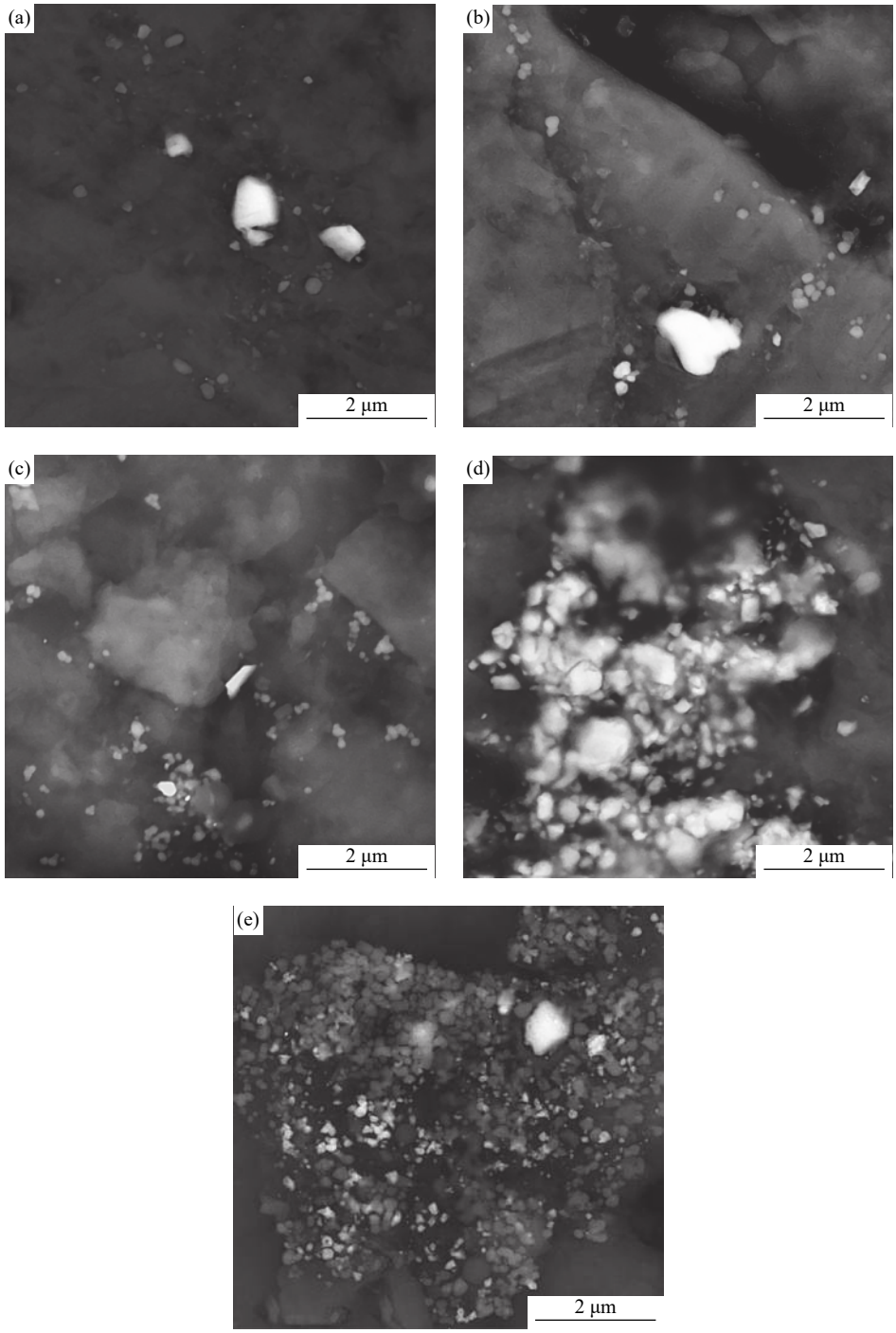

Fig. 4. SEM micrographs of Co_3O_4 nanoparticles distributed in the Al matrix attributed to Al/Co_3O_4 composites with different Co_3O_4 content: (a) 0.5wt%, (b) 1.0wt%, (c) 1.5wt%, (d) 2.0wt%, and (e) 2.5wt%.

composites using SEM. Agglomeration occurred at low concentration of Co_3O_4 nanoparticles. As shown in Figs. 4(a) and 4(b), Co_3O_4 particles became agglomerated and distributed on the particles of the Al matrix at 0.5wt% and 1wt% Co_3O_4. With 1.5wt% Co_3O_4 and more, Co_3O_4 particles accumulated in the interspace of the Al particles, along with agglomeration. The accumulation of Co_3O_4 particles in the interspace of Al particles (Fig. 4(e)) indicates that this placement imparted compressive stress on Al crystals. The quasi-spherical shape of the Al particles was maintained for all samples.

3.3. Vickers hardness analysis

The hardness of the samples is shown in Fig. 5. The

hardness of a compound is an indicator of its resistance against plastic deformation, which can vary by altering the mode and extent of stress and strain exerted on its crystal structure. In this experiment, an increase in the amount of Co_3O_4 and compressive strain of the crystal structure substantially influenced the hardness, increasing from HV 28 to HV 52 with the addition of 2.5wt% Co_3O_4. The addition of Co_3O_4 had two impacts. First, the particles occupied the free interspace of Al particles and consequently resulted in homogenous sintering. Secondly, the creation of a compressive stress on coarser Al particles improved composite hardness. Fathy *et al*. [32] evaluated the influence of the addition of Fe to a Al matrix and reported that the formation of intermetallic phases could also enhance the composite hardness. Since the presence of intermetallic phases in the XRD patterns was not detected in our research, the impact of the phases on the sample hardness is not clear.

3.4. Magnetic behavior of the composites

The VSM results of Al/Co_3O_4 composites are depicted in Fig. 6, and Table 2 summarizes the analysis of the results. Accordingly, the magnetic behavior of the composites as the soft magnetic mode, H_c, was identical for all samples, and

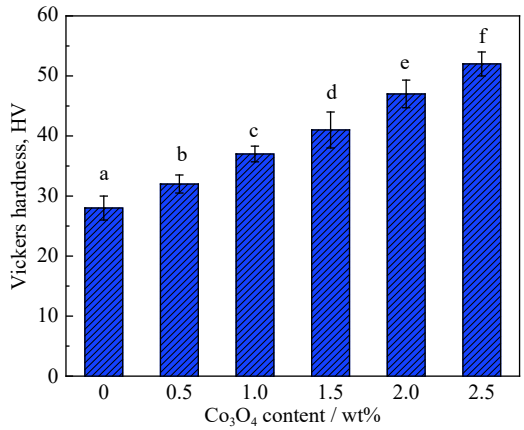

Fig. 5. Hardness of Al/Co_3O_4 composites with different Co_3O_4 nanoparticle content. Bar Charts represent mean (n = 5) ± SD. Different letters on the bars charts represent the significant difference at 5% probability.

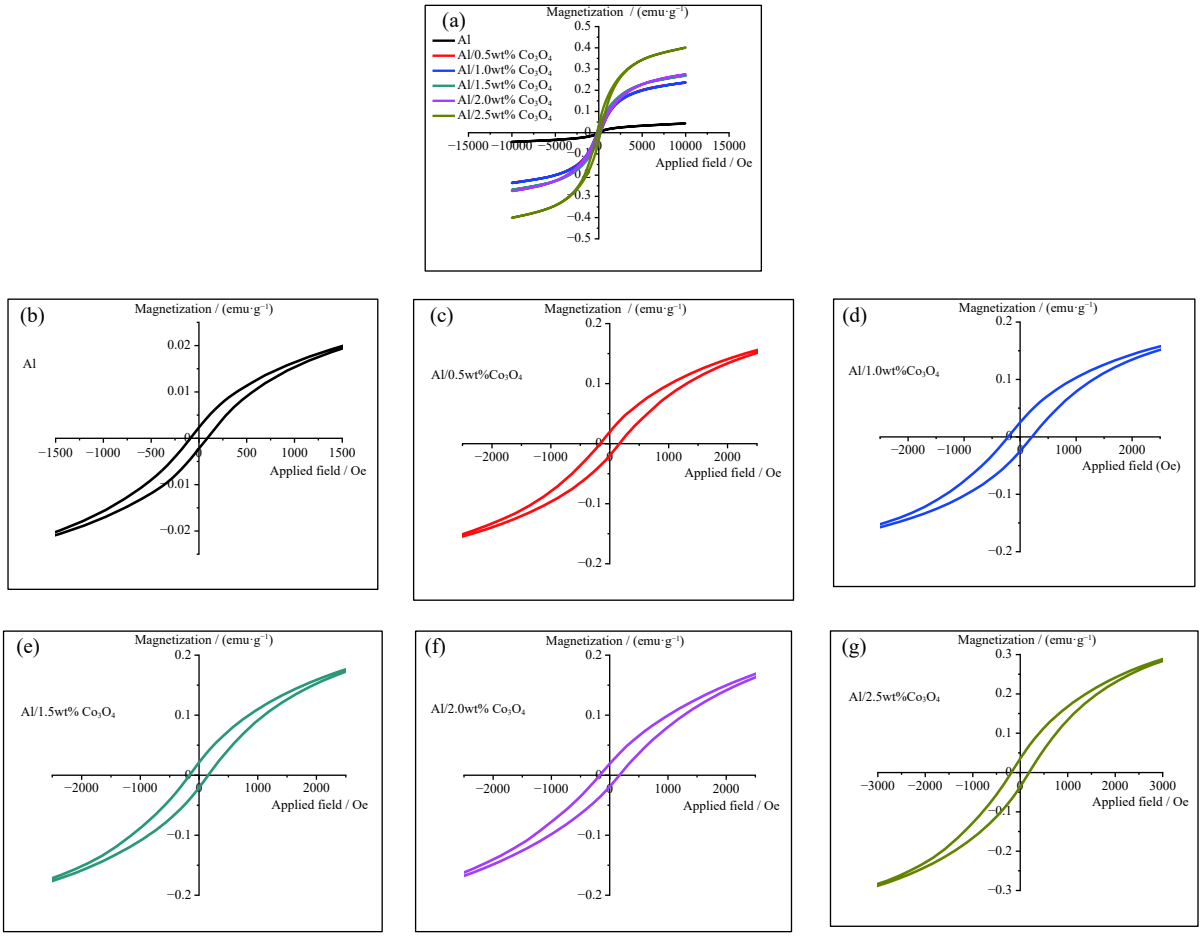

Fig. 6. VSM results of the Al/Co_3O_4 composite for all samples and individual samples with different Co_3O_4 contents: (a) all samples; (b) 0wt%, (c) 0.5wt%, (d) 1.0wt%, (e) 1.5wt%, (f) 2.0wt%, and (g) 2.5wt%.

Table 2. VSM results of Al/Co_3O_4 composite containing different amount of Co_3O_4 (hysteresis loop information belongs to Fig. 6)

Sample	M_s / (emu·g^{-1})	M_r / (emu·g^{-1})	H_c / Oe
Al	0.044 ± 0.01^a	0.00284 ± 0.0003^e	83.31 ± 50.05^h
Al/0.5wt%Co_3O_4	0.236 ± 0.02^b	0.01983 ± 0.002^f	148.97 ± 56.43^h
Al/1.0wt%Co_3O_4	0.237 ± 0.01^b	0.02453 ± 0.003^f	185.48 ± 64.14^h
Al/1.5wt%Co_3O_4	0.269 ± 0.02^c	0.02105 ± 0.002^f	147.73 ± 54.89^h
Al/2.0wt%Co_3O_4	0.275 ± 0.02^d	0.02000 ± 0.001^f	192.75 ± 73.12^h
Al/2.5wt%Co_3O_4	0.401 ± 0.03^d	0.03633 ± 0.003^g	151.06 ± 55.26^h

Note: the data shows mean (n = 5) ± SD. Different letters on the data represent the significant difference at 5% level of probability.

the addition of Co_3O_4 did not result in a significant change, which confirms that the magnetic behavior of the samples is due to the Al particles and are not affected the addition of Co_3O_4.

M_s increased with the incorporation of Co_3O_4 nanoparticles into the Al matrix and increased the structural strain because of the stress imposed by the accumulation of Co_3O_4 particles into the interspace of the Al particles. Compressive structural strains developed in Al particles influenced the magnetic regions and, as a result, increased the magnetic saturation under the predetermined magnetic field. According to Brown's theory [33], an increase in the stress raises magnetization in small level of stress. With increasing stress of the crystal structure, plans and directions of the crystals can be organized in an appropriate orientation thereby enhancing the magnetic behavior [33]. Roskosz *et al.* [27] examined the association between residual stress and the residual magnetic field and found that by exerting uniaxial stress (σ) on the magnetic regions, the magnetic field (H_σ) could impact the residual stress of the evaluated material based on Eq. 3:

$$H_\sigma(\varphi) = \frac{3\sigma}{2\mu_0}\left(\frac{d\lambda}{dM}\right)_T \left(\cos^2\varphi - \nu\sin^2\varphi\right) \quad (3)$$

where σ = stress, λ = magnetostriction, μ_0 = magnetic permeability of free space, M = magnetization, φ = the angle between the stress axis and the direction of magnetic field H_σ, and ν = Poisson's ratio.

This feature can also affect the remanence magnetic (M_r). M_r increased with increasing Co_3O_4 content, which can be attributed to differences in the magnetic regions caused by structural strain and the stability of the regions by the removal of the magnetic field.

In general, the pure Al sample exhibits anti-ferromagnetic behavior but its magnetic behavior turns into ferromagnetic with the addition of Co_3O_4. M. Galini *et al.* [34] reported that bulk Co_3O_4 had an anti-ferromagnetic behavior but nano-Co_3O_4 had weak ferromagnetic features. This alteration can be ascribed to the uncompensated surface spins or finite size impact of the Co_3O_4 nanoparticles. Thus, M_r can be reasonably reduced via the addition of Co_3O_4 to Al.

4. Conclusions

Our observations of the fabrication and evaluation of Al/Co_3O_4 features demonstrate that, although adding Co_3O_4 nanoparticles had no effect on the crystallite size of Al, the accumulation of Co_3O_4 particles into the free interspace of Al particles created compressive strain in their crystalline structure. The compressive strain increased with increasing Co_3O_4 content such that it influenced the composite characteristics. The increased residual compressive strain and accumulation of Co_3O_4 particles in the free interspace of Al particles improved the composite hardness. Although the magnetic behavior of the fabricated composites was only dependent upon the Al particles, the inclusion of Co_3O_4 nanoparticles improved the magnetic saturation and remanence magnetization of the composite. Therefore, the nanoparticles can be used to alter magnetic regions.

References

[1] K.B. Nie, Y.C. Guo, K.K. Deng, and X.K. Kang, Microstructure and mechanical properties of TiCp/Mg–4Zn–0.5Ca nanocomposite in different processing conditions, *Mater. Res. Express*, 6(2019), No. 6, p. 066525.

[2] R. Taherian, M.M. Ghorbani, and S.R. Kiahosseini, A new method for optimal fabrication of carbon composite paper as gas diffusion layer used in proton exchange membrane of fuel cells, *J. Electroanal. Chem.*, 815(2018), p. 90.

[3] O. Güven, S.N. Monteiro, E.A.B. Moura, and J.W. Drelich, Re-emerging field of lignocellulosic fiber–polymer composites and ionizing radiation technology in their formulation, *Polym. Rev.*, 56(2016), No. 4, p. 702.

[4] B.D. Agarwal, L.J. Broutman, and K. Chandrashekhara, *Analysis and Performance of Fiber Composites*, John Wiley & Sons, Rolla, 2017.

[5] E.J. Barbero, *Introduction to Composite Materials Design*, CRC press, Boca Raton, 2017.

[6] M. Taya and R.J. Arsenault, *Metal Matrix Composites*: *Thermomechanical Behavior*, Elsevier, Amsterdam, 1989.

[7] A. Nanni, *Fibre Reinforced-Plastic* (*FRP*) *Reinforcement*

for Concrete Structures: *Properties and Applications*, Elsevier, Amsterdam, 1993.

[8] C.F. Lin, Y.Q. Han, C.H. Guo, Y.P. Chang, X.X. Han, L. Lan, and F.C. Jiang, Synthesis and mechanical properties of novel Ti–(SiC_f/Al_3Ti) ceramic-fiber-reinforced metal-intermetallic-laminated (CFR-MIL) composites, *J. Alloys Compd.*, 722(2017), p. 427.

[9] L. Joyyi, M.Z.A. Thirmizir, M.S. Salim, L.Z. Han, P. Murugan, K. Kasuya, F.H. Maurer, M.I.Z. Arifin, and K. Sudesh, Composite properties and biodegradation of biologically recovered P(3HB-*co*-3HHx) reinforced with short kenaf fibers, *Polym. Degrad. Stab.*, 137(2017), p. 100.

[10] K. Wang, N. Li, J. Zhang, Z.Q. Zhang, and F.Q. Dang, Size-selective QD@MOF core-shell nanocomposites for the highly sensitive monitoring of oxidase activities, *Biosens. Bioelectron.*, 87(2017), p. 339.

[11] J.X. Fan, D.Y. Chen, N.J. Li, Q.F. Xu, H. Li, J.H. He, and J.M. Lu, Adsorption and biodegradation of dye in wastewater with Fe_3O_4@MIL-100 (Fe) core-shell bio-nanocomposites, *Chemosphere*, 191(2018), p. 315.

[12] A. Wagih, Mechanical properties of Al–Mg/Al_2O_3 nanocomposite powder produced by mechanical alloying, *Adv. Powder Technol.*, 26(2015), No. 1, p. 253.

[13] Azimi, A. Shokuhfar, and O. Nejadseyfi, Mechanically alloyed Al7075–TiC nanocomposite: Powder processing, consolidation and mechanical strength, *Mater. Des.*, 66(2015), p. 137.

[14] A.M. Pourrahimi, T.A. Hoang, D.M. Liu, L.K. Pallon, S. Gubanski, R.T. Olsson, U.W. Gedde, and M.S. Hedenqvist, Highly efficient interfaces in nanocomposites based on polyethylene and ZnO nano/hierarchical particles: a novel approach toward ultralow electrical conductivity insulations, *Adv. Mater.*, 28(2016), No. 39, p. 8651.

[15] H. Zhang, S. Hwang, M. Wang, Z. Feng, S. Karakalos, L. Luo, Z. Qiao, X. Xie, C. Wang, and D. Su, Single atomic iron catalysts for oxygen reduction in acidic media: particle size control and thermal activation, *J. Am. Chem. Soc.*, 139(2017), No. 40, p. 14143.

[16] S. Mohapatra, A.K. Chaubey, D.K. Mishra, and S.K. Singh, Fabrication of Al–TiC composites by hot consolidation technique: its microstructure and mechanical properties, *J. Mater. Res. Technol.*, 5(2016), No. 2, p. 117.

[17] V.R. Rao, N. Ramanaiah, and M.M.M. Sarcar, Tribological properties of aluminium metal matrix composites (AA7075 reinforced with titanium carbide (TiC) particles), *Int. J. Adv. Sci. Technol.*, 88(2016), p. 13.

[18] U. Riedel and J. Nickel, Applications of natural fiber composites for constructive parts in aerospace, automobiles, and other areas, [in] *Biopolymers Online,* Epub ahead of print 2005, https://doi.org/10.1002/3527600035.bpola001

[19] S.F. Li, K. Kondoh, H. Imai, B. Chen, L. Jia, J. Umeda, and Y.B. Fu, Strengthening behavior of in situ-synthesized (TiC–TiB)/Ti composites by powder metallurgy and hot extrusion, *Mater. Des.*, 95(2016), p. 127.

[20] X. Gao, H.Y. Yue, E.J. Guo, H. Zhang, X.Y. Lin, L.H. Yao, and B. Wang, Preparation and tensile properties of homogeneously dispersed graphene reinforced aluminum matrix composites, *Mater. Des.*, 94(2016), p. 54.

[21] M. Mansournia and N. Rakhshan, Amine ligand-based hydrothermal synthesis of Co_3O_4 nanoparticles, characterization and magnetic study, *J. Mol. Struct.*, 1125(2016), p. 714.

[22] J. Li, X.L. Zhao, J.P. Liu, L. Zhang, and C.H. Yang, Ultralight carbon-based $Co(OH)_2$ Co_3O_4/nanocomposite with superior performance in wave absorption, *J. Alloys Compd.*, 777(2019), p. 954.

[23] H. Shokrollahi, A review of the magnetic properties, synthesis methods and applications of maghemite, *J. Magn. Magn. Mater.*, 426(2017), p. 74.

[24] Z. Ji, P.H. Ai, C. Shao, T.J. Wang, C.X. Yan, L. Ye, and W. Gu, Manganese-doped carbon dots for magnetic resonance/optical dual-modal imaging of tiny brain glioma, *ACS Biomater. Sci. Eng.*, 4(2018), No. 6, p. 2089.

[25] P. Dutta, M.S. Seehra, S. Thota, and J. Kumar, A comparative study of the magnetic properties of bulk and nanocrystalline Co_3O_4, *J. Phys.*: *Condens. Matter*, 20(2007), No. 1, art. No. 015218.

[26] J. Buršík, M. Soroka, R. Uhrecký, R. Kužel, F. Mika, and Š. Huber, Thin (111) oriented CoFe2O4 and Co_3O_4 films prepared by decomposition of layered cobaltates, *Appl. Surf. Sci.*, 376(2016), p. 209.

[27] M. Roskosz, A. Rusin, and M. Bieniek, Analysis of relationships between residual magnetic field and residual stress, *Meccanica*, 48(2013), No. 1, p. 45.

[28] S.R. Kiahosseini, A. Afshar, M.M. Larijani, and M. Yousefpour, Adhesion, microstrain, and corrosion behavior of ZrN–coated AZ91 alloy as a function of temperature, *J. Mater. Res.*, 28(2013), No. 19, p. 2709.

[29] S.R. Kiahosseini and M.M. Larijani, Effects of nitrogen gas ratio on the structural and corrosion properties of ZrN thin films grown on biodegradable magnesium alloy by ion-beam sputtering, *Appl. Phys. A*, 123(2017), No. 12, p. 759.

[30] S.R. Kiahosseini, A. Afshar, M.M. Larijani, and M. Yousefpour, Structural and corrosion characterization of hydroxyapatite/zirconium nitride-coated AZ91 magnesium alloy by ion beam sputtering, *Appl. Surf. Sci.*, 401(2017), p. 172.

[31] S. Fooladi and S.R. Kiahosseini, Creation and investigation of chitin/HA double-layer coatings on AZ91 magnesium alloy by dipping method, *J. Mater. Res.*, 32(2017), No. 13, p. 2532.

[32] A. Fathy, E.-K. Omyma and M. M. Mohammed, Effect of iron addition on microstructure, mechanical and magnetic properties of Al-matrix composite produced by powder metallurgy route, *Trans. Nonferrous Met. Soc. China*, 25(2015), No. 1, p. 46.

[33] D.J. Craik and M.J. Wood, Magnetization changes induced by stress in a constant applied field, *J. Phys. D*: *Appl. Phys.*, 3(1970), No. 7, p. 1009.

[34] M. Galini, M. Salehi, and M. Behzad, Structural, magnetic and dielectric properties of pure and Dy-doped Co_3O_4 nanostructures for the electrochemical evolution of oxygen in alkaline media, *J. Nanostruct.*, 8(2018), No. 4, p. 391.